2015

Cyclotron production of high–specific activity 55Co and in vivo evaluation of the stability of 55Co metal-chelate-peptide complexes

Tara Mastren
Washington University School of Medicine in St. Louis

Bernadette V. Marquez
Washington University School of Medicine in St. Louis

Deborah E. Sultan
Washington University School of Medicine in St. Louis

Elizabeth Bollinger
Washington University School of Medicine in St. Louis

Paul Eisenbeis
Washington University School of Medicine in St. Louis

See next page for additional authors

RESEARCH ARTICLE

Cyclotron Production of High–Specific Activity ^{55}Co and In Vivo Evaluation of the Stability of ^{55}Co Metal-Chelate-Peptide Complexes

Tara Mastren, Bernadette V. Marquez, Deborah E. Sultan, Elizabeth Bollinger, Paul Eisenbeis, Tom Voller, and Suzanne E. Lapi

Abstract

This work describes the production of high–specific activity ^{55}Co and the evaluation of the stability of ^{55}Co-metal-chelate-peptide complexes in vivo. ^{55}Co was produced via the ^{58}Ni(p,α)^{55}Co reaction and purified using anion exchange chromatography with an average recovery of 92% and an average specific activity of 1.96 GBq/μmol. ^{55}Co-DO3A and ^{55}Co-NO2A peptide complexes were radiolabeled at 3.7 MBq/μg and injected into HCT-116 tumor xenografted mice. Positron emission tomography (PET) and biodistribution studies were performed at 24 and 48 hours postinjection and compared to those of $^{55}CoCl_2$. Both ^{55}Co-metal-chelate complexes demonstrated good in vivo stability by reducing the radiotracers' uptake in the liver by sixfold at 24 hours with ~ 1% ID/g and at 48 hours with ~ 0.5% ID/g and reducing uptake in the heart by fourfold at 24 hours with ~ 0.7% ID/g and sevenfold at 48 hours with ~ 0.35% ID/g. These results support the use of ^{55}Co as a promising new radiotracer for PET imaging of cancer and other diseases.

POSITRON EMISSION TOMOGRAPHY (PET) is a common imaging modality in nuclear medicine. Clinical interest in positron-emitting metals has increased due to their longer half-lives, which are more suitable for radiolabeling macromolecules such as antibodies, peptides, and nanoparticles over traditional PET isotopes such as ^{18}F, ^{11}C, and ^{15}O.[1,2] Currently, the most common radiometals used in PET imaging are ^{64}Cu, ^{68}Ga, ^{89}Zr, and ^{86}Y, with ^{64}Cu, ^{68}Ga, and ^{89}Zr being used in clinical trials.[3–5] The chemistry of each metal is different, and chelates need to be optimized for the radiometal of interest that will provide stable metal-chelate complexes in vivo.

^{55}Co is another isotope of interest for PET imaging. It has a half-life of 17.5 hours, a positron branching ratio of 77%, and an average positron energy of 570 keV, qualities that make it well suited for imaging with peptides, small molecules, and antibodies.[6–11] $^{55}CoCl_2$ has previously been used clinically to image ischemia in stroke patients[12–15] and in late-onset epileptic seizures[16] due to its ability to mimic calcium uptake. However, it is important to study the preclinical pharmacologic properties of this isotope when it will be incorporated into targeting ligands as imaging agents to probe other diseases. Thus, we investigated the biodistribution of free $^{55}CoCl_2$ along with the stability of ^{55}Co-chelate-peptide complexes in vivo.

^{55}Co can be produced via several nuclear reactions, such as ^{58}Ni(p,α)^{55}Co,[17–20] ^{56}Fe(p,2n)^{55}Co,[21,22] and ^{54}Fe(d,n)^{55}Co.[23,24] The ^{54}Fe(d,n)^{55}Co has the highest measured cross section at low energies[8,25]; however, ^{54}Fe has a low natural abundance. Thus, this target may be cost prohibitive for routine production in most laboratories. The ^{56}Fe(p,2n)^{55}Co reaction also creates undesirable ^{56}Co (via ^{56}Fe(p,n)^{56}Co), a positron-emitting isotope with a half-life of 77 days that is chemically inseparable from ^{55}Co. Additionally, the decay scheme for this isotope yields many high-energy photons. The proton reaction on ^{58}Ni has a higher cross section at lower energies than the proton reaction on ^{56}Fe,[19,20,22] making it more desirable for low-energy (15 MeV) cyclotrons. This method also produces a small amount of an inseparable side product, ^{57}Co ($t_{1/2}$ = 271.8 days) at higher energies with a Q value of 8.17 MeV. ^{57}Co decays 100% by electron capture and has a low-energy gamma ray of 122 keV. In addition to ^{57}Co, this method also produces another side product, ^{57}Ni ($t_{1/2}$ = 35.6 hours), which can be used as a way to monitor the separation of ^{55}Co from the starting nickel material by tracking the characteristic gamma rays via gamma spectroscopy.

The production of ^{55}Co using ^{nat}Ni and ^{58}Ni has previously been reported.[11,18,26,27] The specific activity of ^{55}Co

From the Departments of Chemistry and Radiology, Washington University, St. Louis, MO.

Address reprint requests to: Suzanne E. Lapi, Department of Radiology, Washington University, Campus Box 8225, 510 S. Kingshighway Blvd, St. Louis, MO 63110; e-mail lapis@mir.wustl.edu.

DOI 10.2310/7290.2015.00025

DECKER

has been investigated using both ion chromatography of productions using ^{58}Ni[26], and 4,7,10-tetraazacyclododecane-1,4,7,10-tetraacetic acid (DOTA) and 1,4,7-triazacyclononane-1,4,7-triacetic acid (NOTA) titration of productions using ^{nat}Ni.[27] High–effective specific activity (ESA) of radiometals is important, as metal contaminants have negative impacts on radiolabeling.[28,29] For best radiolabeling results using ^{55}Co, ESA measurements must be performed and productions optimized so that high–specific activity material can be obtained.

In this work, we discuss the production of ^{55}Co via the ^{58}Ni(p,α)^{55}Co reaction and report its ESA using both DOTA titrations and ion chromatography.[28] We also report the in vivo biodistribution $^{55}CoCl_2$ and compare it to its ^{55}Co-chelate complexes linked to a peptide up to 48 hours. The macrocyclic chelates DOTA and NOTA were chosen because they meet the coordination chemistry required to bind ^{55}Co. DOTA and NOTA are commonly attached to peptides via one of their carboxylic acid arms, resulting in DO3A- and NO2A-peptide conjugates, respectively.[30,31] As a model system, we applied ^{55}Co to a peptide ligand, L19K-FDNB, which has been shown to have a long blood-clearance time.[32] This property makes this peptide an optimal system for studying the stability of ^{55}Co-chelate complexes as ^{55}Co-DO3A-L19K-FDNB and ^{55}Co-NO2A-L19K-FDNB in vivo at time points up to 48 hours. The biodistribution data for $^{55}CoCl_2$, ^{55}Co-NO2A-L19K-FDNB, and ^{55}Co-DO3A-L19K-FDNB were compared at 24 and 48 hours postinjection to establish the in vivo stability of ^{55}Co chelated with NO2A- and DO3A-peptide conjugates in tumor-bearing mice.

Materials and Methods

Materials

Trace metal grade reagents were purchased from Sigma-Aldrich (St. Louis, MO) and used without purification, and Milli-Q deionized water (18 MΩ cm^{-1}) was used for all dilutions unless stated otherwise. All glassware and vials were acid washed in 8 M HNO_3 for 24 hours prior to use. DOTA was purchased from Macrocyclics (Dallas, TX). Two versions of the peptide L19K were synthesized by CPC Scientific (Sunnyvale, CA) consisting of the sequence DO3A- or NO2A-PEG_4-GGNECDIARMWEWECFERK-$CONH_2$, with a Cys-Cys disulfide bridge and polyethylene glycol (PEG) as a spacer between peptide and chelate. ^{58}Ni was purchased from Isoflex (San Francisco, CA) with 99.48% isotopic enrichment.

Targetry and Irradiation

Forty-five to 55 mg of ^{58}Ni in powder form was plated onto a gold disk by electrodeposition as previously described by McCarthy and colleagues and Szelecsenyi and colleagues.[33,34] The electroplating cell was 9 cm in height, with an inner diameter of 1.8 cm. The bottom of the cell consisted of a Teflon base that connected to the gold disk, exposing a 5 mm circle. A graphite rod was used as the cathode and stirred the solution slowly as a voltage of 2.5 V was applied for ~ 12 hours. The current remained between 8 and 20 mA throughout the process. Targets were irradiated on a 15 MeV cyclotron (CS-15) for 20 to 60 μAhr and were able to withstand currents up to 30 μA. Targets were allowed to sit for 2 hours prior to processing to allow short-lived contaminants to decay.

Purification

For processing, targets were placed in 10 mL of 9 M HCl and heated with reflux for approximately 1 hour to dissolve the nickel from the gold disk. Once the solution cooled, it was placed in a 1 cm × 10 cm glass column (Bio-Rad, Hercules, CA) with 2.5 g AG1-X8 resin (Bio-Rad). To determine separation conditions, the eluate and 10 to 40 mL of 9 M HCl were collected, followed by another 10 mL of 0.5 M HCl to elute the ^{55}Co. Fractions of 1 mL were collected and analyzed using a high-purity germanium (HPGe) detector (Canberra, Meriden, CT), and the final ^{55}Co fractions were evaporated to dryness and reconstituted with 20 μL Milli-Q water. ^{55}Co productions were analyzed using ion chromatography[28] for transition metal contamination.

Effective Specific Activity

DOTA titrations were performed to determine the ESA of ^{55}Co productions, and the method was adapted from the 1,4,8,11-tetraazacyclotetradecane-1,4,8,11-tetraacetic acid (TETA) titration method reported previously by McCarthy and colleagues.[33] Then, 1.2 MBq (5 μL) of ^{55}Co was added to eight different amounts of DOTA in ammonium acetate pH 5.5, ranging from 4.3×10^{-4} μmol to 6.3×10^{-2} μmol. The final volume was brought to 50 μL using 0.5 M ammonium acetate buffer pH 5.5. The solutions were placed in an agitating incubator at 37ºC for 30 minutes. Solutions were cooled to room temperature and then centrifuged. A 1 μL aliquot from each DOTA concentration and 1 μL of unbound ^{55}Co, for use as a control, were spotted separately onto a silica plate for thin-layer chromatography (TLC) using a 1:1 mixture of 10% w/v ammonium acetate and methanol as the eluent. Plates were analyzed using a Radio TLC Plate Reader (Washington, DC) and analyzed for the percent ^{55}Co incorporated into DOTA. Data were plotted as the molar concentration of DOTA versus percent ^{55}Co incorporation. The curve was fit using a sigmoid plot fit program in *Prism*

(GraphPad Software, La Jolla, CA). The EC_{50} value, the concentration of ^{55}Co that bound to 50% of the DOTA molecules, was determined from this fit. The ESA was calculated as two times the EC_{50} value.

Animal Models

All animal care was performed as stated in the *Guide for Care and Use for Laboratory Animals* by the National Institutes of Health under a protocol approved by the Animal Studies Committee at Washington University in St. Louis. Female athymic Nu/Nu mice (National Cancer Institute, Bethesda, MD) age 6 to 9 weeks were anesthetized with a ketamine/xylazine cocktail (VEDCO, St, Joseph, MO). One hundred microliters of approximately 2×10^7 cell/mL HCT-116 colon cancer cells suspended in saline was subcutaneously injected into the shoulder. Tumors were allowed to grow for 2 weeks before imaging and biodistribution studies.

Small Animal PET/CT imaging

Prior to imaging, animals were anesthetized with 2% isoflurane. One hundred microliters of 74 kBq/μL $^{55}CoCl_2$ in saline was injected into HCT-116 tumor–bearing mice ($n = 4$) via tail vein injection and imaged using an Inveon MicroPET/CT scanner (Siemens, Washington, DC) at 2, 24, and 48 hours postinjection. Static PET images were acquired for 20 minutes. PET data were reconstructed using standard methods with the maximum a posteriori probability (MAP) algorithm and coregistered with computed tomography (CT) using image display software (Inveon Research Workplace Workstation, Siemens). Volumes of interest (VOI) were drawn using CT anatomic guidelines.

Biodistributions

^{55}Co-NO2A-L19K-FDNB and ^{55}Co-DO3A-L19K-FDNB were prepared and radiolabeled similarly to the ^{64}Cu analogues described by Marquez and colleagues[32] and with a final specific activity of 3.7 MBq/μg. One hundred microliters of 74 kBq/μL $^{55}CoCl_2$, 37 kBq/μL ^{55}Co-NO2A-FDNB, or 37 kBq/μL ^{55}Co-DO3A-FDNB in saline was injected into HCT-116 tumor–bearing mice. For each agent, three mice were sacrificed at 24 and 48 hours postinjection followed by removal of blood, lung, liver, spleen, kidney, muscle, fat, heart, brain, bone, tumor, stomach, small intestine, upper large intestine, and lower large intestine. Each organ was weighed and measured for radioactivity using a gamma counter. The radioactivity was background subtracted, decay corrected to the time of injection, and reported as percent injected dose/g tissue (% ID/g).

Statistical Analysis

All data were analyzed using *Prism* version 6 and reported as mean ± standard deviation (SD). One-way analysis of variance (ANOVA) was used to calculate p values in order to compare more than two groups with one variable, and p values with a 95% confidence interval ($< .05$) were considered significant.

Results

Production and Purification of High–Specific Activity ^{55}Co

^{58}Ni was plated onto a gold disk with an average efficiency of 95 ± 3% and a thickness of ~ 300 μm. Irradiations produced an average of 6 ± 1 MBq ^{55}Co/μAhr, which is consistent with yields predicted by Kaufman[20] and about 30% lower than yields predicted by Reimer and Qaim.[19] ^{57}Ni and ^{57}Co were coproduced at rates of 16 ± 2 kBq/μAhr and 11 ± 2 kBq/μAhr, respectively, and were approximately 25% and 20% lower than yields predicted by Reimer and Qaim,[19] respectively.

Due to the coproduction of ^{57}Ni, separation could be analyzed by measuring the characteristic gamma rays of ^{57}Ni (E_1 = 1.378 MeV, I_1 = 81.7% and E_2 = 0.127 MeV, I_2 = 16.7%) and ^{55}Co (E_1 = 0.931 MeV, I_1 = 75%; E_2 = 0.477 MeV, I_2 = 20.2%; and E_3 = 1.409 MeV, I_3 = 16.9%) in each fraction using an HPGe detector. Elution profiles for ^{57}Ni and ^{55}Co are shown in Figure 1. ^{57}Co contamination was determined by analyzing its characteristic gamma ray 0.122 MeV (85.6%) in each fraction. Washing the column with an additional 10 to 40 mL 9 M HCl removed nickel without significant loss of ^{55}Co. The average recovery of ^{55}Co with a 40 mL 9 M HCl column wash was 92 ± 3%.

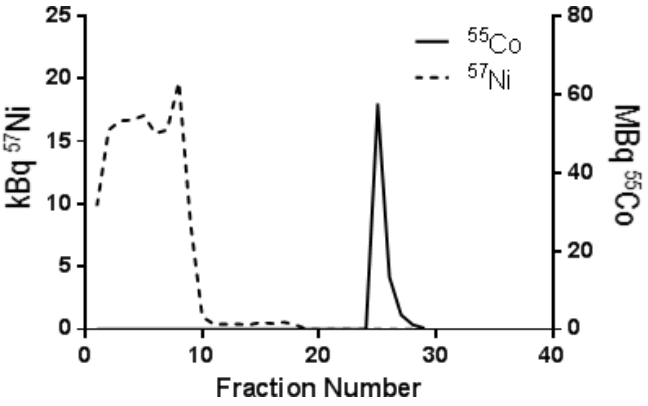

Figure 1. Activity of ^{55}Co and ^{57}Ni in each fraction, as measured using high-purity germanium detection of the characteristic gamma rays, showing good separation.

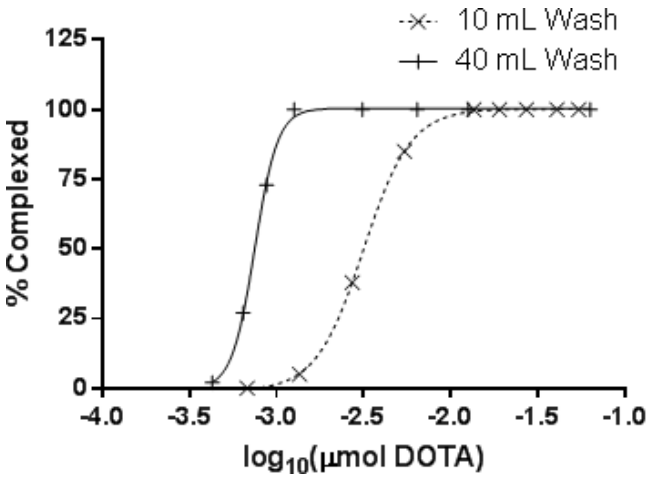

Figure 2. ^{55}Co-DOTA titration curves demonstrating a sevenfold increase in ESA (259 MBq/μmol to 1.96 GBq/μmol) when washing the column with an additional 40 mL 9 M HCl acid versus a 10 mL column wash.

ESA measured via DOTA titration was found to be 259 MBq/μmol DOTA when washing the column with 10 mL 9 M HCl. Increasing the column wash to 40 mL resulted in an increased ESA of 1.96 GBq/μmol DOTA (Figure 2). Ion chromatography measured nickel concentrations to be 94.6 μmol/MBq and 757 nmol/MBq for 10 mL and 40 mL column washes, respectively. The only radioactive impurity found in the final ^{55}Co fraction was ^{57}Co at 0.2% of the total ^{55}Co activity.

$^{55}CoCl_2$ Small Animal PET/CT Imaging and Biodistribution

As an emerging radioisotope applicable in oncologic PET imaging, very few data existed about the in vivo stability of different ^{55}Co-chelate complexes. HCT-116 tumor xenografts were imaged (Figure 3A) and post-PET biodistribution studies (Table 1) were performed at 2, 24, and 48 hours postinjection to investigate the distribution of free $^{55}CoCl_2$ in this model. Interestingly, free $^{55}CoCl_2$ was observed in the tumor at each of these time points. Tumor to blood ratios at 2 and 48 hours were 0.6 ± 0.1 and 1.9 ± 0.4, respectively (p = .006), exhibiting a threefold increase due to fast blood clearance and relatively slow tumor washout (see Figure 3B and Table 1). High uptake in the heart at 2 hours postinjection could be due to the potential of Co^{2+} to mimic calcium influx.[12,15] Clearance of free $^{55}CoCl_2$ occurred through the liver and kidney as indicated by the high uptake values at 2 hours postinjection followed by about a twofold consecutive decrease in $^{55}CoCl_2$ uptake at 24 and 48 hours postinjection (see Table 1).

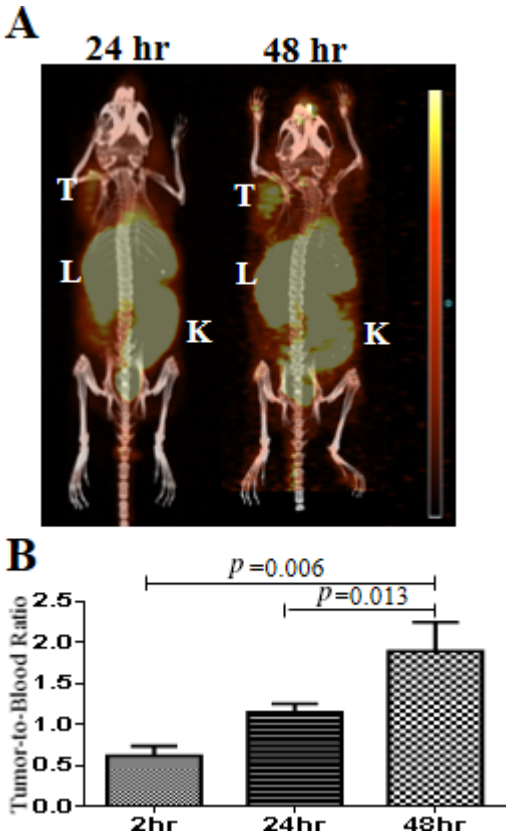

Figure 3. *A*, Twenty-four- and 48-hour PET images of $^{55}CoCl_2$ showing uptake in the tumor and clearance through the liver, kidney, and intestines. *B*, The tumor to blood ratio exhibits a threefold increase from 2 to 48 hours.

Stability of ^{55}Co-Chelate Complexes

The stability of radiometal-chelate combinations is crucial when designing new PET imaging probes. Complexes that are not stable in vivo can lead to the radiometal decomplexing from the chelate and accumulating in different organs throughout the body, increasing background signal and dose to nontarget organs. The longer blood clearance associated with the L19K-FDNB peptide that we chose as our model system to investigate ^{55}Co allows for the potential decomplexation of ^{55}Co-chelate complexes to be measured at clinically relevant time points to evaluate the in vivo stability of these complexes. It has previously been established that changing the radiometal on peptides can have a drastic effect on the affinity of the peptide to its receptor.[35] Using ^{55}Co to radiolabel the NO2A- or DO3A-peptides dramatically decreased the affinity for their tumor-associated target, vascular endothelial growth factor (VEGF),[32] as shown by their reduced tumor uptake compared to the ^{64}Cu-labeled analogue, which was radiolabeled at the same specific activity (Figure S1, online version only).

Table 1. Biodistribution Data for $^{55}CoCl_2$, ^{55}Co-NO2A-L19K-FDNB, and ^{55}Co-DO3A-L19K-FDNB Postinjection

	Postinjection Time						
	2 hr (%ID/g ± SD)	*24 hr (%ID/g ± SD)*			*48 hr (%ID/g ± SD)*		
Organ	*A*	*A*	*B*	*C*	*A*	*B*	*C*
Blood	4.5 ± 0.6	1.40 ± 0.04	1.57 ± 0.09	1.4 ± 0.2	0.46 ± 0.05	0.63 ± 0.09	0.68 ± 0.04
Lung	4.0 ± 0.3	1.9 ± 0.1	0.9 ± 0.1	0.8 ± 0.1	0.98 ± 0.09	0.46 ± 0.06	0.56 ± 0.03
Liver	15.7 ± 0.4	6.2 ± 0.8	1.0 ± 0.1	1.1 ± 0.2	2.7 ± 0.7	0.44 ± 0.03	0.7 ± 0.1
Spleen	1.9 ± 0.4	0.82 ± 0.05	0.6 ± 0.1	0.56 ± 0.08	0.46 ± 0.04	0.37 ± 0.04	0.35 ± 0.03
Kidney	10.5 ± 1.4	4.4 ± 0.4	12.6 ± 4.1	16.0 ± 3.8	1.9 ± 0.2	2.3 ± 1.0	5.8 ± 1.2
Muscle	0.6 ± 0.1	0.37 ± 0.08	0.31 ± 0.04	0.32 ± 0.09	0.17 ± 0.03	0.15 ± 0.02	0.19 ± 0.04
Fat	1.5 ± 0.9	0.7 ± 0.4	0.8 ± 0.4	0.4 ± 0.1	0.23 ± 0.05	0.3 ± 0.1	0.30 ± 0.03
Heart	4.8 ± 0.4	2.8 ± 0.7	0.7 ± 0.1	0.63 ± 0.06	1.4 ± 0.2	0.33 ± 0.04	0.39 ± 0.03
Brain	0.31 ± 0.02	0.17 ± 0.03	0.08 ± 0.06	0.05 ± 0.01	0.11 ± 0.01	0.02 ± 0.01	0.02 ± 0.01
Bone	1.3 ± 0.2	0.8 ± 0.1	0.28 ± 0.04	0.30 ± 0.04	0.5 ± 0.1	0.14 ± 0.02	0.26 ± 0.05
Tumor	2.8 ± 0.6	1.6 ± 0.2	0.9 ± 0.1	1.1 ± 0.2	0.86 ± 0.08	0.49 ± 0.09	0.71 ± 0.03
Stomach	1.1 ± 0.1	1.0 ± 0.2	0.14 ± 0.05	0.22 ± 0.03	0.5 ± 0.1	0.09 ± 0.04	0.12 ± 0.03
Small intestine	3.6 ± 0.6	1.1 ± 0.2	0.26 ± 0.01	0.31 ± 0.04	0.50 ± 0.04	0.14 ± 0.04	0.19 ± 0.03
Upper large intestine	4.3 ± 0.8	1.5 ± 0.1	0.9 ± 0.1	0.8 ± 0.1	0.7 ± 0.1	0.46 ± 0.06	0.56 ± 0.03
Lower large intestine	1.9 ± 1.0	2.2 ± 0.3	1.0 ± 0.1	1.1 ± 0.2	1.2 ± 0.2	0.44 ± 0.03	0.7 ± 0.1

A = $^{55}CoCl_2$; B = ^{55}Co-NO2A-L19K-FDNB; C = ^{55}Co-DO3A-L19K-FDNB.

The 24- and 48-hour biodistribution studies of ^{55}Co-NO2A-L19K-FDNB and ^{55}Co-DO3A-L19K-FDNB were compared to free $^{55}CoCl_2$ (see Table 1). These data show that both NO2A and DO3A chelates radiolabeled with ^{55}Co exhibit good in vivo stability, as shown by their low uptake in the liver, lung, heart, bone, stomach, and small intestine compared to the high uptake of free $^{55}CoCl_2$ in these organs. The difference in uptake is most notable in the liver, where the ^{55}Co-labeled peptides had a sixfold lower uptake than free $^{55}CoCl_2$ at 24 and 48 hours. ^{55}Co-labeled peptides had a fourfold lower uptake than free $^{55}CoCl_2$ in the heart at 24 hours and a sevenfold lower uptake at 48 hours. Although the affinity of this particular peptide was negatively affected by radiolabeling with ^{55}Co, this study shows that DOTA- and NOTA-derived chelates form stable complexes with ^{55}Co in vivo and may be used to investigate other probes that are insensitive to changes in radiometals.

Discussion

The ^{58}Ni(p,α)^{55}Co reaction is an effective route for producing high–specific activity ^{55}Co. Previously, this method was reported using a copper disk[18] as opposed to gold; however, using copper as the target backing material could have a negative effect on the ESA as copper has a high affinity to both NOTA and DOTA chelators and would compete with ^{55}Co for binding. The downside to this reaction is that it has a lower cross section when compared to other radiometals, such as ^{64}Cu and ^{89}Zr, which may limit the availability of this isotope to facilities that have solid target cyclotron capabilities.

The biodistribution of $^{55}CoCl_2$ is comparable to that previously observed for $^{64}CuCl_2$, as both metals are divalent cations and may have similar interactions with transport proteins in vivo.[36–40] The tumor uptake of ^{55}Co is interesting and warrants further investigation. It is possible that its uptake is due to the overexpression of calcium ion channels often found in cancer cells.[41] Several studies have shown the uptake of $^{55}CoCl_2$ in ischemic cells, and this is believed to be due to ^{55}Co partially mirroring calcium influx.[12,15]

The in vivo stability of the NOTA and DOTA analogues, NO2A and DO3A, complexed with ^{55}Co provides the foundation for developing ^{55}Co-labeled peptides, antibodies, nanoparticles, and small molecules. ^{55}Co-NOTA and ^{55}Co-DOTA complexes have significantly lower liver uptake when compared to ^{64}Cu-NOTA and ^{64}Cu-DOTA complexes (see Table 1),[7,42] which could be beneficial in cases where reduced background signal is desired; that is, liver metastases. The lower liver uptake observed with the ^{55}Co complexes implies that the transchelation problem that exists with ^{64}Cu[42–44] is greatly reduced with the use of ^{55}Co. This reduction in transchelation for the cobalt complexes is in agreement with the transfer half-life of 800 hours for Co from Co(DOTATOC) in human blood serum measured by Heppeler and colleagues.[7] Additionally, the high positron

branching ratio (four times that of ^{64}Cu and three times that of ^{89}Zr) leads to similar images with a lower amount of radioactivity administered. One drawback, however, is the higher dose to nontarget tissue from the additional gamma rays present from the decay of ^{55}Co.

Since the affinity of some peptides is dependent on the attached radiometal, it would be interesting to examine this effect on different peptide models. The anti-VEGF peptide used in this work exhibited lower tumor uptake than previously measured with ^{64}Cu (see Figure S1, online version only); however, in work done by Heppeler and colleagues, ^{55}Co-DOTATOC showed higher affinity for the somatostatin type 2 receptor than any other radiometals measured.[7] These different studies imply that ^{55}Co may also coordinate with the peptide probe concurrently with the chelate to elicit a change in the peptide's affinity for its target. Therefore, determining the structure-activity relationship of these peptide-chelate-metal complexes would be significant for designing superior PET imaging probes.

Conclusions

^{55}Co can be made with high specific activity via the ^{58}Ni(p,α)^{55}Co reaction. The in vivo stability of ^{55}Co-labeled NOTA and DOTA derivatives makes this radioisotope a promising isotope for many different applications. Future work should compare the affinity of ^{55}Co-labeled peptides to other radiometals to optimize the best metal-chelate-peptide combination for the application.

Acknowledgments

We would like to acknowledge Patricia Margenau and Bill Margenau for operation of the CS15 cyclotron. The studies presented in this work were conducted in the MIR Pre-Clinical Pet-CT Facility of the Washington University School of Medicine.

Financial disclosure of authors: This work was performed with support from the Siteman Cancer Center Small Animal Imaging Core under grant number P30 CA91842. This work was supported in part by Department of Energy grant number DESC0007352.

Financial disclosure of reviewers: None reported.

References

1. Ikotun OF, Lapi SE. The rise of metal radionuclides in medical imaging: copper-64, zirconium-89 and yttrium-86. Future Med Chem 2011;3:599–621, doi:10.4155/fmc.11.14.
2. Brasse D, Nonat A. Radiometals: towards a new success story in nuclear imaging?. Dalton Trans 2015;44:4845–58, doi:10.1039/c4dt02911a.
3. Anderson CJ, Ferdani R. Copper-64 radiopharmaceuticals for PET imaging of cancer: advances in preclinical and clinical research. Cancer Biother Radiopharm 2009;24:379–93, doi:10.1089/cbr.2009.0674.
4. Dijkers EC, Oude Munnink TH, Kosterink JG, et al. Biodistribution of 89Zr-trastuzumab and PET imaging of HER2-positive lesions in patients with metastatic breast cancer. Clin Pharmacol Ther 2010;87:586–92, doi:10.1038/clpt.2010.12.
5. Ambrosini V, Campana D, Bodei L, et al. ^{68}Ga-DOTANOC PET/CT clinical impact in patients with neuroendocrine tumors. J Nucl Med 2010;51:669–73, doi:10.2967/jnumed.109.071712.
6. Mirzaii M, Kakavand T, Talebi M, Rajabifar S. Electrodeposition iron target for the cyclotron production of Co-55 in labeling proteins. J Radioanalyt Nucl Chem 2012;292:261–7, doi:10.1007/s10967-011-1399-x.
7. Heppeler A, Andre JP, Buschmann I, et al. Metal-ion-dependent biological properties of a chelator-derived somatostatin analogue for tumour targeting. Chemistry 2008;14:3026–34, doi:10.1002/chem.200701264.
8. Thisgaard H, Olesen ML, Dam JH. Radiosynthesis of Co-55- and Co-58m-labelled DOTATOC for positron emission tomography imaging and targeted radionuclide therapy. J Labelled Comp Radiopharm 2011;54:758–62, doi:10.1002/jlcr.1919.
9. Goethals P, Volkaert A, Vandewielle C, et al. Co-55-EDTA for renal imaging using positron emission tomography (PET): a feasibility study. Nucl Med Biol 2000;27:77–81, doi:10.1016/S0969-8051(99)00077-3.
10. Karanikas G, Schmaljohann J, Rodrigues M, et al. Examination of Co-complexes for radiolabeling of platelets in positron emission tomographic studies. Thromb Res 1999;94:111–5, doi:10.1016/S0049-3848(98)00204-7.
11. Ferreira CL, Lapi S, Steele J, et al. ^{55}Cobalt complexes with pendant carbohydrates as potential PET imaging agents. Appl Radiat Isot 2007;65:1303–8, doi:10.1016/j.apradiso.2007.06.003.
12. De Reuck J, Santens P, Keppens J, et al. Cobalt-55 positron emission tomography in recurrent ischaemic stroke. Clin Neurol Neurosurg 1999;101:15–8, doi:10.1016/S0303-8467(98)00076-6.
13. Stevens H, Jansen HML, De Reuck J, et al. ^{55}Cobalt (Co) as a PET-tracer in stroke, compared with blood flow, oxygen metabolism, blood volume and gadolinium-MRI. J Neurol Sci 1999;171:11–8, doi:10.1016/S0022-510X(99)00229-4.
14. De Reuck J, Santens P, Strijckmans K, Lemahieu I. European Task Force on Age-Related White Matter Changes. Cobalt-55 positron emission tomography in vascular dementia: significance of white matter changes. J Neurol Sci 2001;193:1–6, doi:10.1016/S0022-510X(01)00606-2.
15. De Reuck J, Stevens H, Jansen H, et al. The significance of cobalt-55 positron emission tomography in ischemic stroke. J Stroke Cerebrovasc Dis 1999;8:17–21, doi:10.1016/S1052-3057(99)80034-2.
16. De Reuck J, Vonck K, Santens P, et al. Cobalt-55 positron emission tomography in late-onset epileptic seizures after thrombo-embolic middle cerebral artery infarction. J Neurol Sci 2000;181:13–8, doi:10.1016/S0022-510X(00)00382-8.
17. Brinkman GA, Helmer J, Lindner L. Nickel and copper foils as monitors for cyclotron beam intensities. Radiochem Radioanalyt Lett 1977;28:9–19.
18. Spellerberg S, Reimer P, Blessing G, et al. Production of ^{55}Co and ^{57}Co via proton induced reactions on highly enriched ^{58}Ni. Appl Radiat Isot 1998;49:1519–22, doi:10.1016/S0969-8043(97)10119-1.
19. Reimer P, Qaim SM. Excitation functions of proton induced reactions on highly enriched Ni-58 with special relevance to the production of Co-55 and Co-57. Radiochim Acta 1998;80:113–20, doi:10.1524/ract.1998.80.3.113.

20. Kaufman S. Reactions of protons with 58-nickel and 60-nickel. Phys Rev 1960;117:1532–8, doi:10.1103/PhysRev.117.1532.
21. Al-Abyad M, Comsan MN, Qaim SM. Excitation functions of proton-induced reactions on ^{nat}Fe and enriched ^{57}Fe with particular reference to the production of 57Co. Appl Radiat Isot 2009;67:122–8, doi:10.1016/j.apradiso.2008.07.006.
22. Jenkins IL, Wain AG. Excitation functions for bombardment of Fe-56 with protons. J Inorgan Nucl Chem 1970;32:1419–1425, doi:10.1016/0022-1902(70)80628-5.
23. Sharma H, Zweit J, Smith AM, Downey S. Production of cobalt-55, a short-lived, positron emitting radiolabel for bleomycin. Appl Radiat Isot 1986;37:105–9, doi:10.1016/0883-2889(86)90055-9.
24. Coetzee PP, Peisach M. Activation cross-sections for deuteron-induced reactions on some elements of first transition series, up to 5.5 MeV. Radiochim Acta 1972;17:1–6, doi:10.1524/ract.1972.17.1.
25. Zavorka L, Simeckova E, Honusek M, Katovsky K. The activation of Fe by deuterons at energies up to 20 MeV. J Korean Phys Soc 2011;59:1961–4, doi:10.3938/jkps.59.1961.
26. Mastren T, Sultan D, Lapi SE. Production and separation of Co-55 via the Ni-58(p,alpha)Co-55 reaction. AIP Conf Proc 2012;1509: 96–100, doi:10.1063/1.4773948.
27. Valdovinos HF, Graves S, Barnhart T, Nickles RJ. Co-55 separation from proton irradiated metallic nickel. AIP Conf Proc 2014;1626: 217–20, doi:10.1063/1.4901397.
28. Mastren T, Guthrie J, Eisenbeis P, et al. Specific activity measurement of (6)(4)Cu: a comparison of methods. Appl Radiat Isot 2014;90:117–21, doi:10.1016/j.apradiso.2014.03.016.
29. Zeng D, Anderson CJ. Rapid and sensitive LC-MS approach to quantify non-radioactive transition metal impurities in metal radionuclides. Chem Commun (Camb) 2013;49:2697–9, doi:10.1039/c3cc39071c.
30. De Leon-Rodriguez LM, Kovacs Z. The synthesis and chelation chemistry of DOTA-peptide conjugates. Bioconjug Chem 2008; 19:391–402, doi:10.1021/bc700328s.
31. Studer M, Meares CF. Synthesis of novel 1,4,7-triazacyclononane-N,N′,N″triacetic acid derivatives suitable for protein labeling. Bioconjug Chem 1992;3:337–41, doi:10.1021/bc00016a013.
32. Marquez BV, Ikotun O, Meares CF, Lapi SE. Development of a radiolabeled irreversible peptide (RIP) as a PET imaging agent for vascular endothelial growth factor. J Labelled Comp Radiopharm 2013;56:1029–1034, doi:10.2967/jnumed.113.130898.
33. McCarthy DW, Shefer RE, Klinkowstein RE, et al. Efficient production of high specific activity Cu-64 using a biomedical cyclotron. Nucl Med Biol 1997;24:35–43, doi:10.1016/S0969-8051(96)00157-6.
34. Szelecsenyi F, Blessing G, Qaim SM. Excitation-functions of proton-induced nuclear-reactions on enriched Ni-61 and Ni-64—possibility of production of no-carrier-added Cu-61 and Cu-64 at a small cyclotron. Appl Radiat Isot 1993;44:575–80, doi:10.1016/0969-8043(93)90172-7.
35. Ginj M, Maecke HR. Radiometals of interest for peptide labeling and labeling approaches. In: Sigel H, editor. Metal ions in biological systems. Volume 42: Metal complexes in tumor diagnosis and as anticancer agents. New York: CRC Press; 2004, 116–123.
36. Jorgensen JT, Persson M, Madsen J, Kjaer A. High tumor uptake of Cu-64: implications for molecular imaging of tumor characteristics with copper-based PET tracers. Nucl Med Biol 2013;40:345–50, doi:10.1016/j.nucmedbio.2013.01.002.
37. Zhang HY, Cai HW, Lu X, et al. Positron emission tomography of human hepatocellular carcinoma xenografts in mice using copper (II)-64 chloride as a tracer. Acad Radiol 2011;18:1561–8, doi:10.1016/j.acra.2011.08.006.
38. Qin CX, Liu HG, Chen K, et al. Theranostics of malignant melanoma with (CuCl2)-Cu-64. J Nucl Med 2014;55:812–7, doi: 10.2967/jnumed.113.133850.
39. Kim KI, Jang SJ, Park JH, et al. Detection of increased ^{64}Cu uptake by human copper transporter 1 gene overexpression using PET with $^{64}CuCl_2$ in human breast cancer xenograft model. J Nucl Med 2014;55:1692–8, doi:10.2967/jnumed.114.141127.
40. Peng FY, Lutsenko S, Sun XK, Muzik O. Positron emission tomography of copper metabolism in the Atp7b(−/−) knock-out mouse model of Wilson's disease. Mol Imaging Biol 2012;14: 70–8, doi:10.1007/s11307-011-0476-4.
41. Li M, Xiong Z-G. Ion channels as targets for cancer therapy. Int J Physiol Pathophysiol Pharmacol 2011;3:156–66.
42. Zhang Y, Hong H, Engle JW, et al. Positron emission tomography imaging of CD105 expression with a ^{64}Cu-labeled monoclonal antibody: NOTA is superior to DOTA. Plos One 2011;6:e28005, doi:10.1371/journal.pone.0028005.
43. Kumar SR, Gallazzi FA, Ferdani R, et al. In vitro and in vivo evaluation of ^{64}Cu-radiolabeled KCCYSL peptides for targeting epidermal growth factor receptor-2 in breast carcinomas. Cancer Biother Radiopharm 2010;25:693–703, doi:10.1089/cbr.2010.0820.
44. Bass LA, Wang M, Welch MJ, Anderson CJ. In vivo transchelation of copper-64 from TETA-octreotide to superoxide dismutase in rat liver. Bioconjug Chem 2000;11:527–32, doi:10.1021/bc990167l.

Cyclotron Production of High–Specific Activity ^{55}Co and In Vivo Evaluation of the Stability of ^{55}Co Metal-Chelate-Peptide Complexes

Tara Mastren, Bernadette V. Marquez, Deborah E. Sultan, Elizabeth Bollinger, Paul Eisenbeis, Tom Voller, and Suzanne E. Lapi

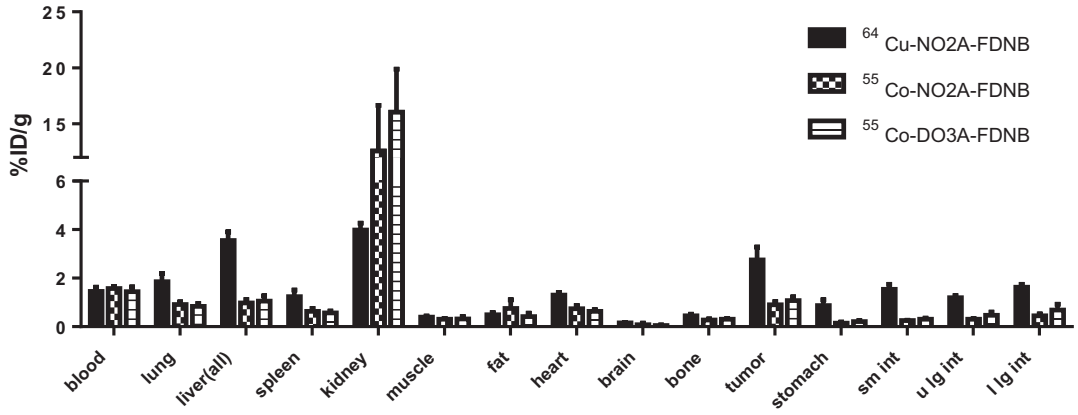

Figure S1. ^{64}Cu-NO2A-FDNB, ^{55}Co-NO2A-FDNB, and ^{55}Co-DO3A-FDNB biodistribution at 24 hours showing significantly higher tumor uptake when using ^{64}Cu over ^{55}Co. ID = injected dose; l lg int = lower large intestine; sm int = small intestine; u lg int = upper large intestine.

From the Departments of Chemistry and Radiology, Washington University, St. Louis, MO.

Address reprint requests to: Suzanne E. Lapi, Department of Radiology, Washington University, Campus Box 8225, 510 S. Kingshighway Blvd, St. Louis, MO 63110; e-mail lapis@mir.wustl.edu.

DOI 10.2310/7290.2015.00025